IFUSP/P-28

DISINTEGRATION OF ^{12}C, ^{19}F, ^{35}Cl, ^{63}Cu and ^{65}Cu BY REAL AND VIRTUAL RADIATION

E.Wolynec, G. Moscati, J.R.Moreira, O.D. Gonçalves* and M.N.Martins*

Instituto de Física

Universidade de São Paulo

* Supported by Fundação de Amparo a Pesquisa do Estado de São Paulo - FAPESP

ABSTRACT

Yield curves were measured for one neutron emission in ^{12}C, ^{19}F, ^{35}Cl and ^{65}Cu, and for two neutron emission in ^{63}Cu, with target stacks which were bombarded by electrons. The results were analyzed to compare the yields from the direct effect of the electrons with those resulting from bremsstrahlung from the eletrons. The analysis was carried out with the virtual photon method in PWBA and DWBA. Agreement with DWBA predictions is obtained assuming photoabsorption through E1 transitions.

SUMÁRIO

Foram medidas as curvas de ativação, para emissão de um neutron, do ^{12}C, ^{19}F, ^{35}Cl e ^{65}Cu e, para emissão de dois neutrons, do ^{63}Cu, bombardeando alvos com electrons. Os resultados foram analisados de forma a comparar as ativações resultantes do efeito direto dos eletrons com as que resultam do bremsstralung dos eletrons. A análise foi efetuada usando o método dos fotons virtuais em PWBA e DWBA. Foi obtido acordo com as previsões de DWBA supondo-se que a fotoabsorção se processa através de transições E1.

1. Introduction

The direct interaction of the electromagnetic field of fast eletrons with nuclear charges and currents is closely related to the interaction of photons with nuclei. When a photon is absorbed by a nucleus the momentum transfer is fixed by the photon energy, whereas when an electron transfers energy to a nucleus the momentum transfer has a continuous distribution. To the approximation that nuclear size can be neglected, the relative effects of photons and electrons in producing nuclear reactions can be evaluated without the detailed knowledge of nuclear wave functions. The only information needed is the multipole order of nuclear transitions involved. By relating the cross-section for electron-nucleus excitation to the corresponding photo excitation process a virtual radiation spectrum can be defined: [1]

$$N^{(\lambda L)}(E_1,w)\ \frac{dw}{w} = \frac{\sigma_e^{\lambda}\ (L,E_1,w)}{\sigma_\gamma^{\lambda}\ (L,w)} \qquad (1)$$

where:

λ = label either E or M for electric or magnetic transitions;

L = multipole order

σ_e = cross-section for electron-nucleus excitation (integrated over all scattering angles);

σ_γ = cross-section for photon-nucleus excitation;

w = photon energy (real or virtual);

E_1 = incident electron total energy

$N^{(\lambda L)}$ = virtual photon intensity spectrum

From (1), the total inelastic electron scattering cross-section may be expressed in a form similar to the yield in photoexcitation experiments:

$$\sigma_e(E_1) = \int_o^{E_1-m_e} \frac{dw}{w} \sum_{\lambda L} \sigma_\gamma^\lambda (L,w) N^{(\lambda L)}(E_1,w) \qquad (2)$$

Thus, expression (2) enables one to evaluate the electroexcitation cross-section, from the photoexcitation cross-section, $\sigma_\gamma^\lambda (L,w)$.

Using plane waves (PW) for the incoming and outgoing electrons, Thie et al.[1] obtained expressions for $N^{(\lambda L)}(E_1,w)$ in the case of E1, E2 and M1 transitions:

For E1 the expression is:

$$N_{PW}^{E1}(E_1,w) = (\alpha/\pi) \left\{ \left[(E_1^2+E_2^2)/(E_1^2-m_e^2) \right] \log \left[(E_1E_2+\sqrt{(E_1^2-m_e^2)} \times \right.\right.$$
$$\left.\left. \times \sqrt{(E_2^2-m_e^2)} - m_e^2)/m_e w \right] - 2 \sqrt{(E_2^2-m_e^2)/(E_1^2-m_e^2)} \right\} \qquad (3)$$

where:

$E_2 = E_1 - w$

m_e = electron's rest energy

α = fine structure constant

Using a distorted wave treatment (DW) with Dirac-Coulomb wave functions for the basis states of the electron, Gargaro and Onley[2], obtained computable expressions for $N^{(\lambda L)}$ for all multipole orders:

$$N_{DW}^{(\lambda L)}(E_1,w) = \left[(\alpha/\pi)(p_1/p_2)(E_1+m_e)(E_2+m_e)w^4(2L+1)^{-1}\right] \kappa_1^{\Sigma}\kappa_2 \quad S(\lambda) \times$$

$$\times (2j_1+1)(2j_2+1) \times \left|C(j_1,j_2,L;\ \frac{-1}{2},\ \frac{1}{2})\ R^{(\lambda)}(\kappa_1,L,\kappa_2)\right|^2 \qquad (4)$$

where:

$p_1(p_2)$ = initial (final) electron momentum;

$S(\lambda)$ = projection operator which retains only those terms satisfying the selection rules for electric or magnetic transitions of multipole order L;

$R^{(\lambda)}$ and remaining parameters are defined in ref.[2]

Experiments [3-7] comparing photo and electrodisintegration of nuclei have been reported. These experiments were carried out before the distorted wave treatment of virtual photon spectra[2] was available.

For light and medium weight nuclei the results of these experiments could be explained, in the plane wave approach, by assuming a mixture of E1 with up to 12% E2 contribution. For high Z the required E2 contribution was of the same magnitude or higher than the E1. A reanalysis of the above data with a

distorted wave treatment[8] showed that they can be explained assuming only E1 transitions. For some of these experiments only 3 or 4 points were measured. The measurements near the threshold show, in general, disagreement with the predictions of both plane and distorted waves treatment.

With the aim of extending data to compare with the theoretical predictions, we carried out measurements of photo and electrodisintegration in some light and medium weight nuclei. The reactions studied are: a) one neutron emission from ^{12}C, ^{19}F, ^{35}Cl, and ^{65}Cu and b) two neutrom emission from ^{63}Cu.

2. Measurements and Analysis

We used the three-foil stack method, for comparing the electro and photodisintegration cross-sections, first described by Brown and Wilson[3]. In this method, a beam of monoenergetic electrons strikes, in succession, a front target, a radiator for producing a known bremsstrahlung spectrum,and finally a back target as identical as possible to the front one. The foil thicknesses are chosen so that the activity N_1, in the front target,is mainly due to electrodesintegration, while that of the back, N_2, is caused by electrodesintegration and photodisintegration in approximately equal amounts. Neglecting the corrections due to the finite thickness of the stack the ratio $(N_2-N_1)/N_1$ would give directly the relative photo to electrodisintegration yields (Y_{Br}/Y_e).

The electron beam was provided by the Linear Accelerator of the Instituto de Física da Universidade de São Paulo. The electron beam passed through a SEM (secondary emission monitor) before striking the targets placed in a vacuum chamber. For each bombardment the SEM current was recorded in a time sequenced scaler (TSS) so that acurate corrections for the decay during bombardments could be made.

The activities of the targets were measured by detecting in coincidence the energy-selected annihilation radiation in two NaI scintillation counters. The targets were often interchanged and counted in the same system. The coincidence pulses were stored in a multichannel analyser operating in TSS, so that the desired initial activities could be obtained by analysis of the decay curves into their components.

For ^{12}C and ^{19}F we used Teflon (C_nF_{2n}) targets and for ^{35}Cl we used PVC (C_3H_5Cl) targets, which also furnished data on ^{12}C. For ^{63}Cu and ^{65}Cu we used natural Copper targets. The radiator was ^{27}Al with a thickness of .546 g/cm^2 (2.28×10^{-2} R.L.) The targets were typically 5×10^{-3} R.L. for PVC, 2×10^{-3} R.L. for Teflon and 5×10^{-3} R.L. for Copper.

In correcting for the finite foil thickness we have used the methods described by Barber:[6]

$$R_{exp} = Y_{Br}/Y_e = R(E_1 - (1/2)\,\Delta_t) =$$

$$= R' \left\{ 1 - R' \left[\frac{(1/2)\,t_t + t_f}{t_t + t_r} \right] \right\}^{-1} \qquad (5)$$

where:

$$R' = \left\{ N_2(E_1)(1- (1/2)\langle\theta^2\rangle) + \left[\frac{\partial(N_1(E_1) + N_2(E_1))}{\partial E_1}\right] \times \right.$$

$$\left. \times \frac{(\Delta_t + \Delta_r)}{2} - N_1 \right\} N_1^{-1} \qquad (6)$$

$N_1(E_1)$ = activity (or yield) per electron induced in the first target foil

$N_2(E_1)$ = activity (or yield) per electron in the target which is behind the radiator

t_t, t_r and t_f = thickness in radiation lenghts of the target, radiator and material upstream from the foil stack, respectively

Δ_t, Δ_r = electron energy loss by radiation and collision in the target and radiator, respectively

$\langle \theta^2 \rangle$ = mean square scattering angle of the electrons in the radiator.

In order to determine the correction term $D=\partial(N_1+N_2)/\partial E_1$ a polynomial of degree n, $P_n(E_1)$ was adjusted to the experimental (N_1+N_2) data. Then, $D = P'_n(E_1) = dP_n(E_1)/dE_1$. The uncertainty in D was evaluated as:

$$(\Delta D)_{rms} = \sqrt{\sum_{i=1}^{n}\sum_{j=1}^{n} \frac{\partial P'_n}{\partial a_i} \frac{\partial P'_n}{\partial a_j} (H_{ij}^{-1})} \,. \qquad (7)$$

where:

$$P_n = \sum_{i=1}^{n+1} a_i x^{i-1}$$

H_{ij} = error matrix for the coefficients of P_n'

The n chosen was the one which gave the best χ^2 with a non-oscilatory solution for the fit. In all cases $2 \leq n \leq 4$.

3. Results and comparison with theory

Figs. 1 to 5 shows the ratios of photo to electro-disintegration presented in units of $(Z_r^2\ r_o^2\ N_r)$, Z_r being the atomic number of the radiator, r_o the classical electron radius and N_r is the number of atoms/cm^2 in the effective radiator. In these units the ratios are called F and become independent of N_r. The errors are a statistical combination of estimated errors incurred in separating the decay curves into their constituent activities and from uncertainty in the corrections. The largest contribution to the total error comes from the uncertainty in D. For a few points near threshold the uncertainty in D was as high as 100%, decreasing typically to about 10% in the steep part of the yield curve.

The ratios predicted by theory are evaluated from:

$$R_{th} = \frac{N_r \int_o^{E_1 - m_e} \sum_{\lambda L} \sigma_\gamma^\lambda (L,w)\ \phi\ (E_1,w,Z_r)\ \frac{dw}{w}}{\int_o^{E_1 - m_e} \sum_{\lambda L} \sigma_\gamma^\lambda (L,w)\ N^{(\lambda L)}(E_1,w)\ \frac{dw}{w}} \qquad (8)$$

where ϕ is the thin target bremsstrahlung intensity spectrum produced in the effective radiator.

In order to compare our experimental data with theory we assumed that the measured photo cross-sections were excited entirely by electric dipole. The curves labelled F_{PW} and F_{DW} in Figs. 1 to 5 were evaluated from the expressions:

$$F_{PW}^{(El)} = (N_r/Z_r^2\ r_o^2\ N_r)\ \frac{\int_o^{E_1-m_e} \sigma_\gamma(w)\ \phi\ (E_1,w,Z_r)\ \frac{dw}{w}}{\int_o^{E_1-m_e} \sigma_\gamma(w)\ N_{PW}^{El}\ (E_1,w)\ \frac{dw}{w}} \qquad (9)$$

$$F_{DW}^{(El)} = (N_r/Z_r^2\ r_o^2\ N_r)\ \frac{\int_o^{E_1-m_e} \sigma_\gamma(w)\ \phi\ (E_1,w,Z_r)\ \frac{dw}{w}}{\int_o^{E_1-m_e} \sigma_\gamma(w)\ N_{DW}^{El}(E_1,w,Z_t)\frac{dw}{w}} \qquad (10)$$

where, N_{PW}^{El} is given in expression (3), ϕ is the Schiff bremsstrahlung spectrum for intermediate screening[9], σ_γ is the measured photo disintegration cross-section and N_{DW}^{El} is given by an analytical expression which fits the calculations of Gargaro and Onley[2] for $\lambda = E$ and L=1 [10]

$$N_{DW}^{El}\ (E_1,w,Z_t) = N_{PW}^{El}\ (E_1,w) + w\left[1.29\times10^{-5}\exp(1.245Z_t^{1/3} - .052E_1)\right] \times$$

$$\times\ (E_2+m_e)/(E_1+m_e) \qquad (11)$$

where Z_t is the target atomic number. In evaluating expressions (9) and (10) we have used, for σ_γ, data available in the literature [11-14].

The dashed curve in each figure, with its respective χ^2, is the result of fitting a polynomial to experimental data.

For ^{12}C, fig.1, F_{PW} and F_{DW} are almost the same and experimental data is compatible with both. For the other nuclei studied, figs. 2 to 5, experimental data are in good agreement with the distorted wave predictions for electric dipole transitions. This can be seen by the χ^2 values of the DW curves, which reflect how well the theoretical predictions fit the measured points(no free parameters adjusted).

4. Conclusions

From the presented data and its analysis we can conclude that the DW calculation, based on the formalism of Gargaro and Onley, explains the experimental results, assuming photoabsorption through E1 transitions, even near the threshold.

ACKNOWLEDGEMENTS

We acknowledge Dr. J.Goldemberg and Dr.D.S.Onley for useful discussions.

REFERENCES

1. J.A.Thie, C.J.Mullin and E.Guth, Phys.Rev. 87, 962 (1952).

2. W.W.Gargaro and D.S.Onley, Phys. Rev. C4, 1032 (1971)

3. K.L.Brown and R.W.Wilson, Phys. Rev. 93, 443 (1954)

4. M.B.Scott, A.O.Hanson and D.W.Kerst, Phys. Rev. 100, 209 (1956)

5. R.L.Hines, Phys. Rev. 105, 1534 (1957)

6. W.C.Barber, Phys.Rev. 111, 1642 (1958)

7. W.C.Barber and T. Wiedling, Nucl.Phys. 18, 575 (1960)

8. E.Wolinec, G.Moscati, O.D.Gonçalves and M.N.Martins
(to be published)

9. H.W.Koch and J.W.Motz, Rev. Mod.Phys. 31, 920 (1959)

10. E.Wolynec et al. (to be published)

11. J.D.King, R.N.H.Haslam and W.J. McDonald, Can.J.Phys. 38, 1069 (1960)

12. S.C.Fultz, J.T.Caldwell, B.L.Bermam. R.L.Bramblett and R.R.Harvey, Phys.Rev. 143, 790 (1966)

13. S.C.Fultz, R.L.Bramblett, J.T.Caldwell and R.R.Harvey, Phys. Rev. 133, B1149 (1964)

14. F.Ferrero, S.Ferroni, R.Malvano, S.Menardi and E.Silva, Nuovo Cimento 11, 410 (1959).

FIGURE CAPTIONS

Fig. 1 - Measured F for $^{12}C(\gamma,n)$. The full circles and triangles refer to our measurements with Teflon and PVC targets, respectively. Full squares are data from ref.[6]. Dashed curve is a polynomial fitting to the points. Full curves are F_{PW} and F_{DW} predictions.

Fig. 2 - Measured F for $^{19}F(\gamma,n)$. Dashed curve is a polynomial fitting to the points. Full curves are F_{PW} and F_{DW} predictions.

Fig. 3 - Measured F for $^{35}Cl(\gamma,n)$. Dashed curve is a polynomial fitting to the points. Full curves are F_{PW} and F_{DW} predictions.

Fig. 4 - Measured F for ^{65}Cu (γ,n). Dashed curve is a polynomial fitting to the points. Full curves are F_{PW} and F_{DW} predictions.

Fig. 5 - Measured F for ^{63}Cu $(\gamma,2n)$. Dashed curve is a polynomial fitting to the points. Full curves are F_{PW} and F_{DW} predictions.

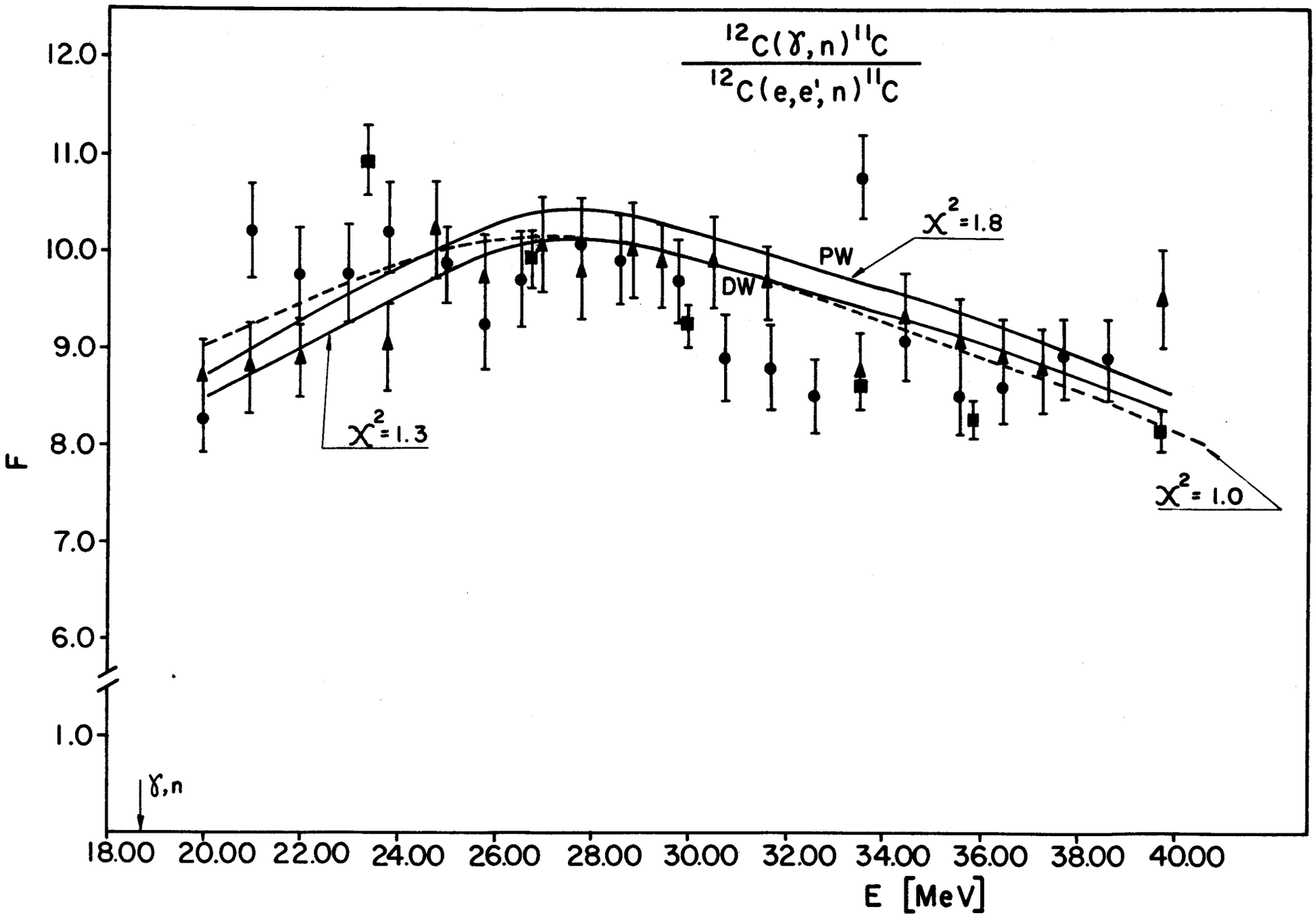
$\frac{^{12}C(\gamma,n)^{11}C}{^{12}C(e,e',n)^{11}C}$
12.0
11.0
10.0
9.0
8.0
7.0
6.0
1.0
F
χ^2=1.8
PW
DW
χ^2=1.3
χ^2=1.0
γ,n
18.00
20.00
22.00
24.00
26.00
28.00
30.00
32.00
34.00
36.00
38.00
40.00
E [MeV]

figure 1

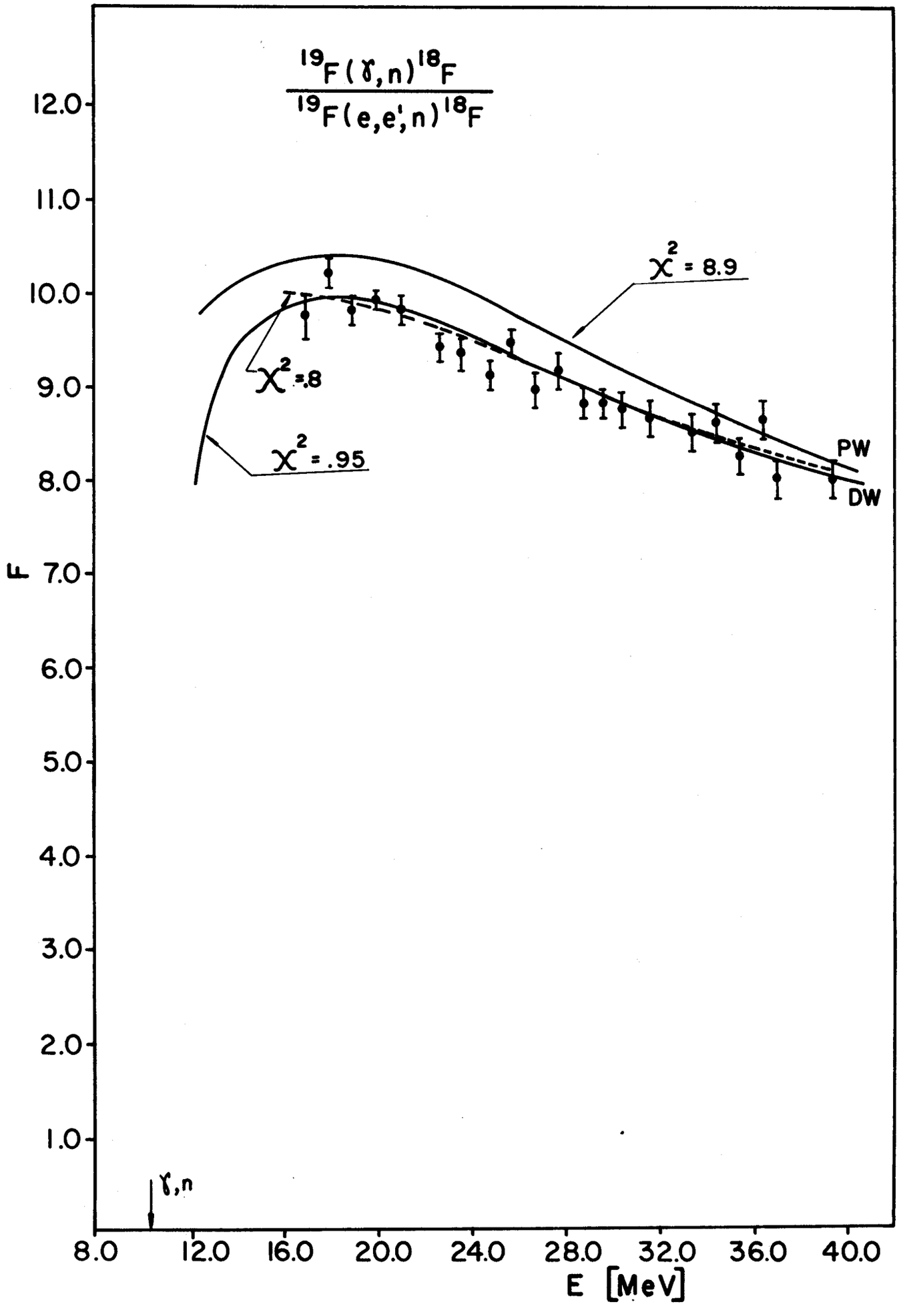
$\frac{^{19}F(\gamma,n)^{18}F}{^{19}F(e,e',n)^{18}F}$
12.0
11.0
10.0
9.0
8.0
7.0
6.0
5.0
4.0
3.0
2.0
1.0
F
$\chi^2 = 8.9$
$\chi^2 = .8$
$\chi^2 = .95$
PW
DW
γ,n
8.0
12.0
16.0
20.0
24.0
28.0
32.0
36.0
40.0
E [MeV]

figure 2

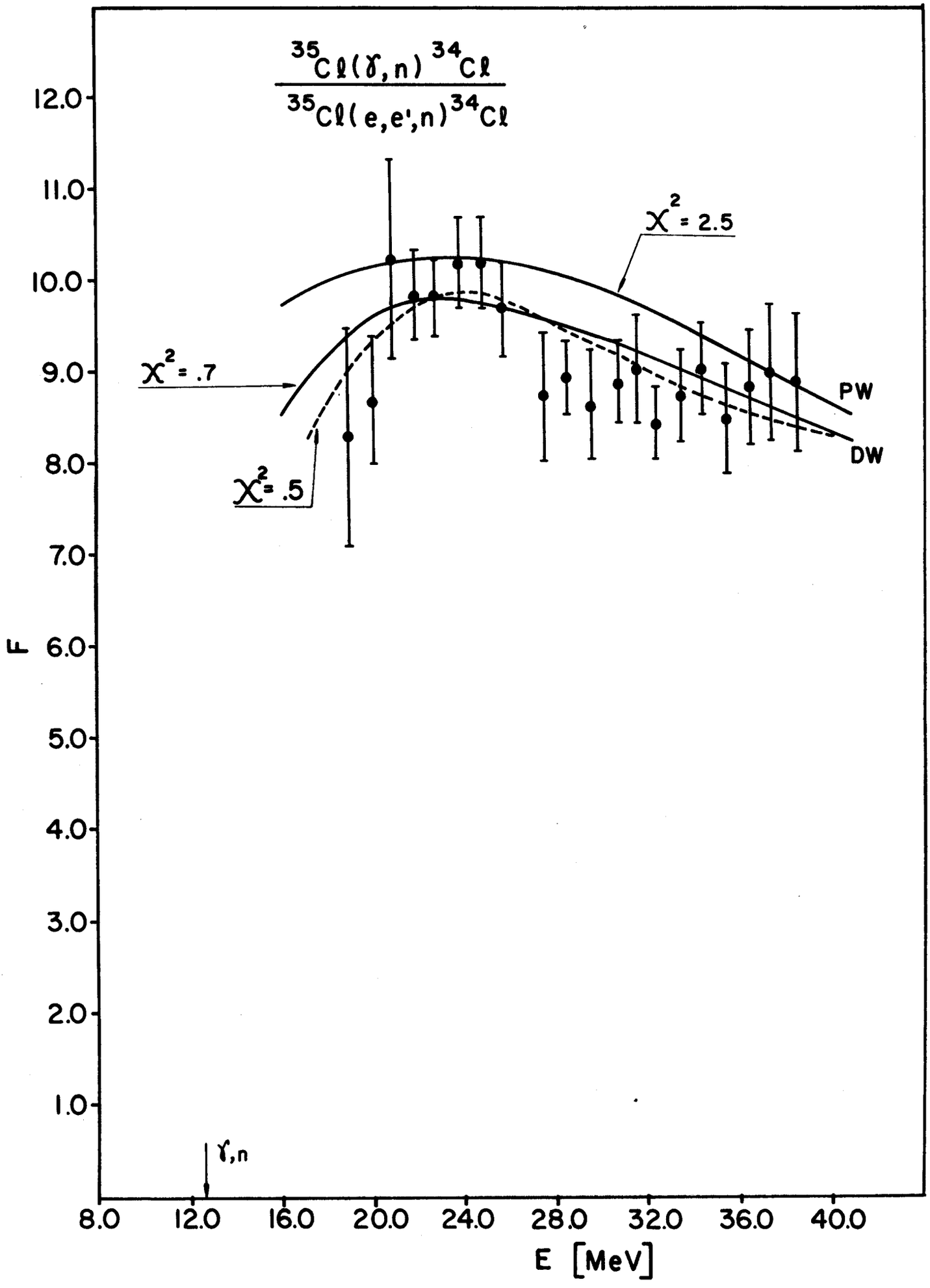
$^{35}Cl(\gamma,n)^{34}Cl$ / $^{35}Cl(e,e',n)^{34}Cl$
$\chi^2 = 2.5$
$\chi^2 = .7$
$\chi^2 = .5$
PW
DW
F
E [MeV]
γ,n
12.0
11.0
10.0
9.0
8.0
7.0
6.0
5.0
4.0
3.0
2.0
1.0
8.0
12.0
16.0
20.0
24.0
28.0
32.0
36.0
40.0

figure 3

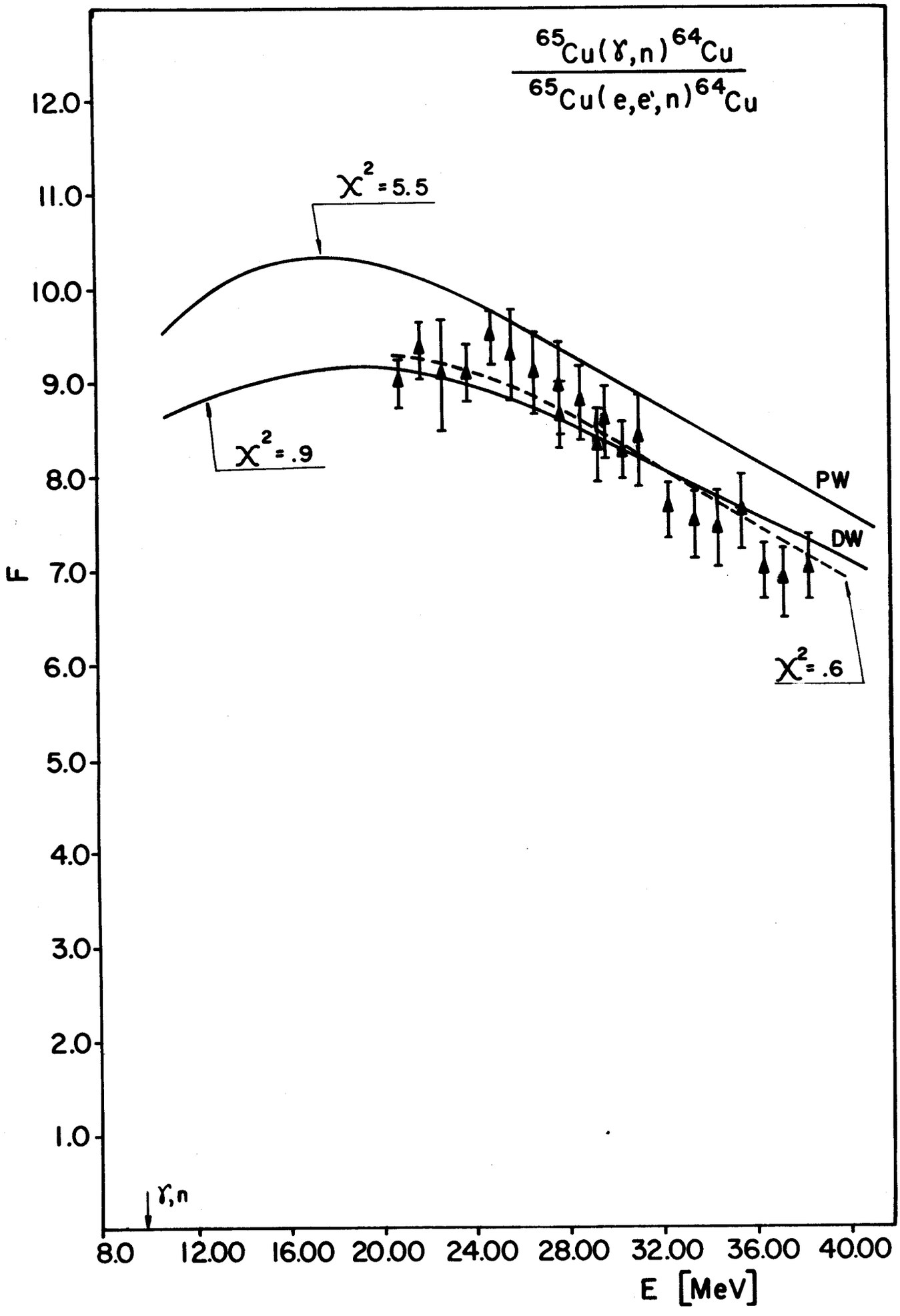
$^{65}Cu(\gamma,n)^{64}Cu$ / $^{65}Cu(e,e',n)^{64}Cu$
$\chi^2 = 5.5$
$\chi^2 = .9$
$\chi^2 = .6$
PW
DW
F
12.0
11.0
10.0
9.0
8.0
7.0
6.0
5.0
4.0
3.0
2.0
1.0
γ,n
8.0
12.00
16.00
20.00
24.00
28.00
32.00
36.00
40.00
E [MeV]

figure 4

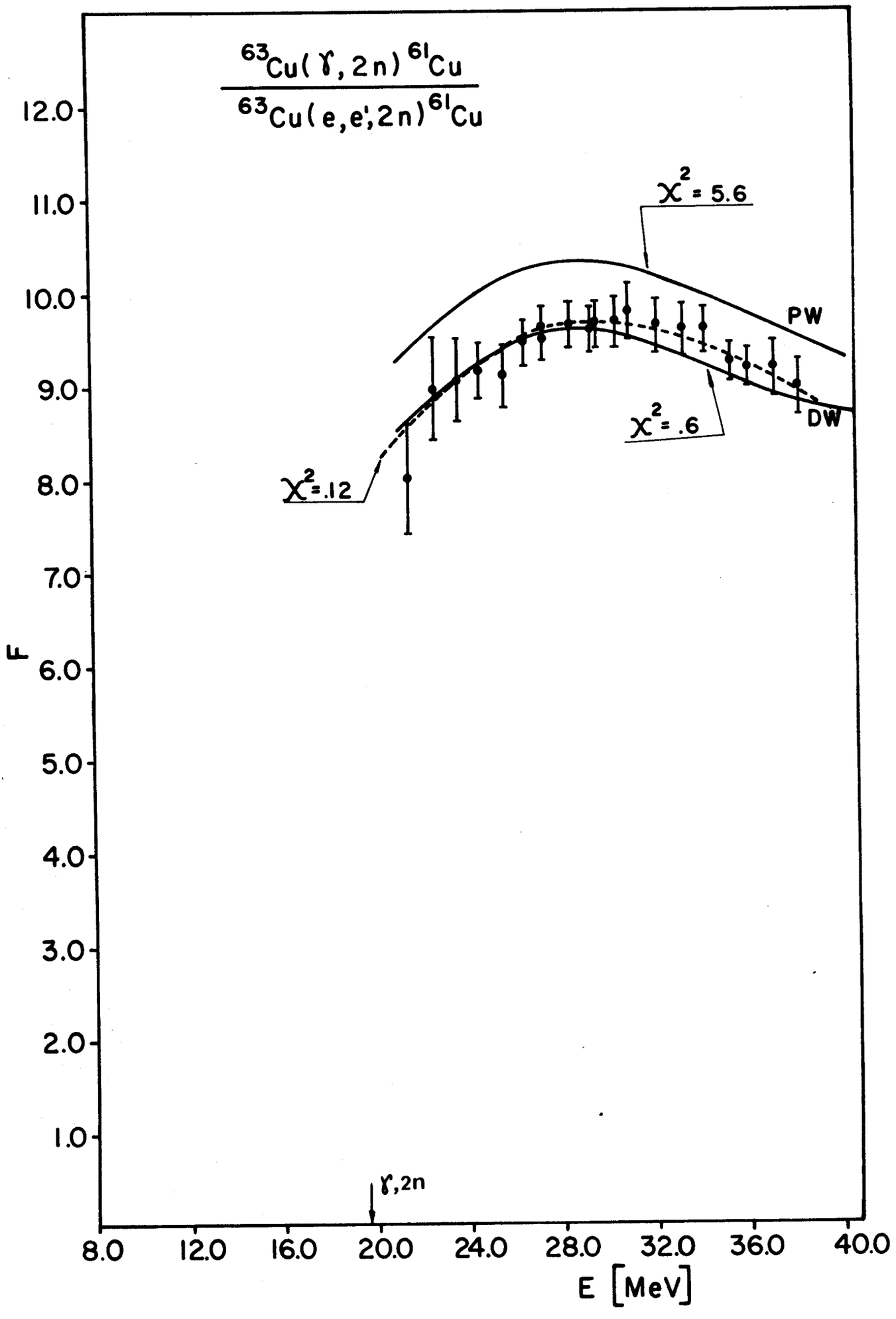
$^{63}Cu(\gamma, 2n)^{61}Cu$
$^{63}Cu(e, e', 2n)^{61}Cu$
$\chi^2 = 5.6$
PW
DW
$\chi^2 = .6$
$\chi^2 = .12$
F
12.0
11.0
10.0
9.0
8.0
7.0
6.0
5.0
4.0
3.0
2.0
1.0
γ,2n
8.0
12.0
16.0
20.0
24.0
28.0
32.0
36.0
40.0
E [MeV]

figure 5